A Compact, Low-Profile Simultaneous Transmit and Receive Antenna With Monopole-Like Radiation Characteristics

Di Wu [ID], *Member, IEEE*, Yuzhang Zang, *Student Member, IEEE*, Hung Luyen [ID], *Member, IEEE*, Mingjian Li [ID], *Member, IEEE*, and Nader Behdad [ID], *Fellow, IEEE*

Abstract—A compact, vertically polarized simultaneous transmit and receive (STAR) antenna with a high transmit–receive isolation level and an omnidirectional radiation pattern in the azimuth plane is presented. The proposed STAR antenna consists of transmit (TX) and receive (RX) antennas whose phase centers are collocated. The TX antenna is a monopole with top-hat loading, placed directly below the central point of the crossed loop. The RX antenna consists of a pair of orthogonal half-loops, each capacitively fed at both of its ends with a $180°$ phase difference. The four ports of the RX antenna are fed with the same amplitude and relative phase values of $0°$, $90°$, $180°$, and $270°$ to produce an omnidirectional radiation pattern and high isolation with the TX antenna. The STAR antenna was designed for operation in the 2.45 GHz ISM band with electrical dimensions of $D \times H = 0.44\lambda \times 0.15\lambda$ (diameter $\times$ height). A prototype of this antenna was fabricated and experimentally characterized. Measurement results show that the antenna has a TX/RX isolation level better than 38 dB and maintains monopole-like patterns for both TX and RX modes over a frequency range of 2.4–2.7 GHz.

Index Terms—In-band full duplex (IBFD), isolation, omnidirectional pattern, self-interference cancellation, simultaneous transmit and receive (STAR) antenna.

I. INTRODUCTION

IN-BAND full-duplex (IBFD) systems have the potential for enhancing the spectrum efficiency of next-generation wireless communication networks [1]. For an IBFD system, signals can be transmitted and received simultaneously at the same frequency, hence doubling the spectral efficiency and system capacity [1]. One of the most challenging works in designing an IBFD system is to suppress self-interference (SI) between the transmit (TX) and receive (RX) chains to a level below the receiver's noise floor [1], [2]. For a typical ISM radio system transmitting at 20 dBm with a receiver noise floor of -90 dBm, an isolation level of more than 110 dB between the TX and RX chains is required [2]. This high isolation can be realized in three different stages: antenna cancellation, radio frequency (RF) interference cancellation, and digital baseband interference cancellation [3]. High isolation in antenna cancellation stage could alleviate the burden of implementing the subsequent RF and digital cancellation stages.

Antenna cancellation for IBFD systems can be realized by using spatial duplexing [4], polarization diversity [5]–[8], resonators placed between the antenna elements for decoupling [9]–[11], four-arm spiral antenna for ultrawideband circular polarization [12]–[14], and near-field cancellation technique [15]–[17]. Among these techniques, the near-field cancellation technique is especially attractive as it allows TX and RX antennas to have not only high isolation but also similar radiation characteristics, especially the polarization and the shape of the radiation patterns along the direction(s) of maximum radiation. In [15], an antenna system with an eight-element TX monopole array distributed on a ring and a centrally located RX monopole was designed for the 2.45 GHz ISM band. To decrease the coupling between each TX element and the RX antenna, the authors used a conductive cylinder with the diameter of 0.84λ and height of 0.62λ, where λ is the free-space wavelength at 2.45 GHz, to elevate the RX antenna. This makes the overall dimensions of the whole antenna system (excluding the ground plane) relatively large as $D \times H = 1.34\lambda \times 0.87\lambda$ (diameter $\times$ height) [16]. In [17], it is shown that the conductive cylinder in this design can be removed to make the antenna more compact with the dimensions of $D \times H = 0.74\lambda_{max} \times 0.25\lambda_{max}$, where λ_{max} is the wavelength at the lowest operating frequency of the antenna.

In this letter, a compact, low-profile, high-isolation simultaneous transmit and receive (STAR) antenna with omnidirectional radiation patterns and vertical polarization for both the RX and TX channels is presented. The proposed, compact STAR antenna is expected to be suitable for several applications including WiFi, vehicle-to-vehicle, as well as military communications [18]. Our proposed STAR antenna architecture consists of a pair of capacitively coupled, orthogonal half-loops as the RX antenna, and a centrally located, top-hat monopole as the TX antenna. The TX antenna is directly fed by a 50 Ω SMA connector. Each half-loop of the RX antenna is differentially fed at

D. Wu was with the Department of Electrical and Computer Engineering, University of Wisconsin-Madison, Madison, WI 53706 USA, and also with the Department of Electrical and Electronic Engineering, The University of Hong Kong, Hong Kong. He is now with the College of Electronic Science and Technology, Shenzhen University, Shenzhen 518060, China (e-mail: diwu0916@gmail.com).

Y. Zang, H. Luyen, and N. Behdad are with the Department of Electrical and Computer Engineering, University of Wisconsin-Madison, Madison, WI 53706 USA (e-mail: yzang5@wisc.edu; luyen@wisc.edu; behdad@wisc.edu).

M. Li was with the Department of Electrical and Computer Engineering, University of Wisconsin-Madison, Madison, WI 53706 USA. He is now with Aptiv, Agoura Hills, CA 91301 USA (e-mail: leeguru@gmail.com).

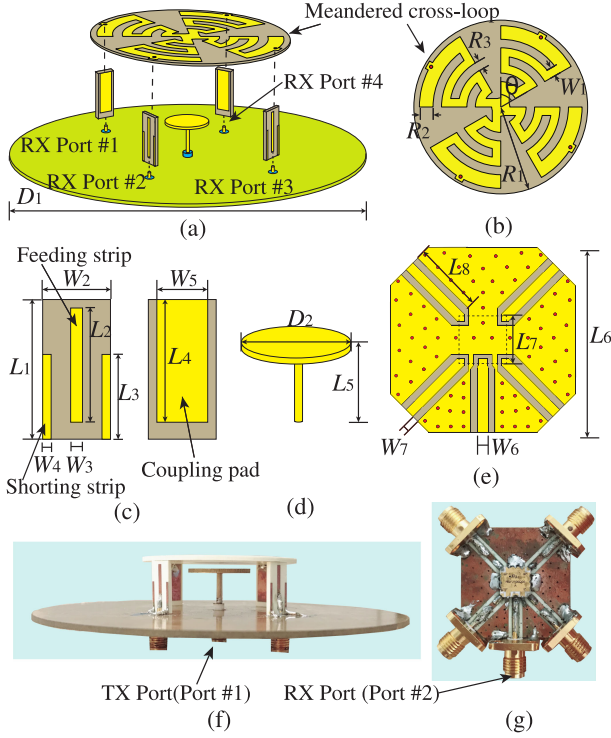Digital Object Identifier 10.1109/LAWP.2019.2898220

Fig. 1.   Geometry of the proposed STAR antenna. (a) 3-D view. (b) Top view of the horizontal portion of the RX antenna. (c) Vertical portion of the RX antenna. (d) TX antenna. (e) Layout of the feeding network of the RX antenna. (f) Photograph of the fabricated STAR antenna. (g) Photograph of the fabricated feeding network used to feed the RX antenna. The physical dimensions of the proposed STAR antenna are listed as follows: $D_1 = 123.00$ mm, $R_1 = 26.29$ mm, $R_2 = 4.21$ mm, $R_3 = 2.61$ mm, $W_1 = 2.62$ mm, $\theta = 60°$, $L_1 = 16.48$ mm, $L_2 = 13.48$ mm, $L_3 = 10.00$ mm, $L_4 = 14.48$ mm, $W_2 = 8.00$ mm, $W_3 = 1.40$ mm, $W_4 = 1.00$ mm, $W_5 = 6.00$ mm, $D_2 = 22.00$ mm, $L_5 = 10.93$ mm, $L_6 = 29.00$ mm, $L_7 = 3.00$ mm, $L_8 = 11.38$ mm, $W_4 = 1.75$ mm, and $W_7 = 1.02$ mm.

both of its ends. The four ports of the RX antenna are connected to a quadrifilar and excited with the same amplitude and linear progressive phase of 90° to generate a near-field null at the location of the TX antenna. Hence, high isolation between the TX and RX antennas can be achieved. Additionally, the horizontal portion of the cross loop is meandered to reduce the height and aperture area of the RX antenna while maintaining vertically polarized radiation. The proposed STAR antenna, excluding the ground plane, has a compact size of $0.44\lambda \times 0.15\lambda$ $(D \times H)$. The volume occupied by this antenna (defined as a cylindrical volume of $\pi \times \frac{D^2}{4} \times H$) is approximately 53 times smaller than that of the STAR antenna operating at the same 2.45 GHz ISM band reported in [15] and [16]. The fabricated prototype exhibits more than 38 dB isolation between the TX and RX ports over the frequency range of 2.4–2.7 GHz, which covers the 2.45 GHz ISM band and maintains consistent, monopole-like patterns for both TX and RX modes over the entire band of operation.

II. ANTENNA DESIGN

Fig. 1 shows the topology of the proposed STAR antenna that comprises a pair of orthogonal, capacitively coupled half-loops acting as the RX antenna and a top-hat loaded monopole acting as the TX antenna. The TX and RX antennas are mounted on a circular ground plane with a diameter of 123 mm and
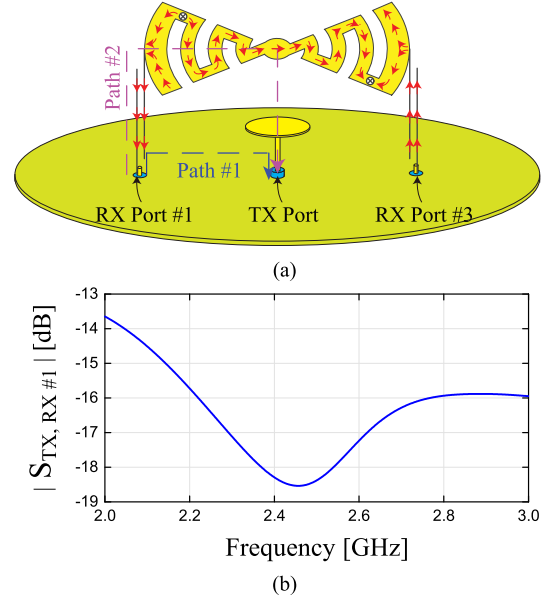

Fig. 2.   (a) Current distributions and mutual coupling paths when RX Ports #1 and #3 are excited with differential signals, whereas the TX Port is loaded with 50 Ω. (b) Mutual coupling between RX port #1 and the TX port.

a thickness of 1.5 mm, as shown in Fig. 1(a). Fig. 1(b)–(d) shows the top view of the cross loop, side views of capacitively coupled feed structures for the RX antenna, and the perspective view of the central TX monopole, respectively. Fig. 1(e) shows the layout of the feeding network of the RX antenna and a dashed rectangular box indicating the footprint of a commercial quadrifilar IC (RFMW RQF2500Q06). The quadrifilar IC is used to excite the four input ports of the RX antenna with equal amplitudes and phases of 0°, 90°, 180°, and 270°. Photographs of the fabricated prototypes of the STAR antenna and the feeding network of the RX antenna are shown in Fig. 1(f) and 1(g), respectively. The antenna was designed to work in the ISM frequency band (2.4–2.5 GHz). The physical dimensions of the proposed STAR antenna are provided in Fig. 1.

A. TX Antenna Design

The TX antenna is a top-hat loaded monopole located at the center of the ground plane and aligned with the vertical symmetry axis of the RX antenna, as shown in Fig. 1(d). The top hat of the TX antenna not only reduces the profile of the TX monopole antenna, but also contributes to the coupling path #2 to reduce the mutual coupling between each RX port and the TX port, as shown in Fig. 2(a). The height of the monopole and diameter of the top hat were optimized in full-wave simulations that take into account the presence of the RX antenna to achieve good impedance matching for the TX antenna over the operating frequency range of 2.4–2.5 GHz. The final dimensions for the diameter of the top hat and height of the monopole are 22 and 10.93 mm, respectively.

B. RX Antenna Design

The RX antenna consists of two orthogonal loops, as shown in Fig. 1(a). The total length of each loop, measured from RX port #1 to #3 or from RX port #2 to #4, is about one wavelength

at 2.45 GHz. The four ports of the RX antenna are capacitively fed to make each port well matched to 50 Ω. The geometry of each capacitively coupled feed structure is shown in Fig. 1(c), which consists of a central feeding strip and two grounding strips on one side of a dielectric substrate, and a coupling pad on the other side of the substrate. The central feeding strip is connected to the inner conductors of an SMA connector, and the coupling pad is directly connected to the meandered cross loop. By using the two grounding strips, the impedance matching of each RX port could be further improved. The capacitive feed structures and meandered cross loop are implemented on Rogers RO4350B substrates, with a permittivity of 3.48 and a thickness of 1.524 mm.

The four ports of the RX antenna are fed with the same amplitudes and different phase values of $0°$, $90°$, $180°$, and $270°$, respectively. The distance R_1 between each RX port to the center of the ground plane is 26.29 mm, equivalent to 0.22λ, where λ is the free-space wavelength at 2.45 GHz. This distance is small enough to ensure a relatively omnidirectional radiation pattern can be obtained [17]. In addition, since the opposing ports of each loop are fed with the same amplitude and $180°$ phase difference, a near-field null is created on the central axis of the RX array where the TX monopole is placed. This helps achieve a high isolation level between the TX and RX antennas [15]–[17].

The horizontal portion of the cross loop is meandered to reduce the dimensions of the STAR antenna. As a result, the STAR antenna has a very compact size of $D \times H =$ 52.6 mm $\times$ 18.5 mm, excluding the ground plane. Indeed, the volume of the proposed STAR antenna is about 98.1% smaller compared to that of a prominent STAR antenna design utilizing the near-field cancellation technique reported in [15] and [16] while having similar bandwidth. The use of the meandered cross loop also allows for reducing the distances between the RX ports and hence, resulting in a more omnidirectional radiation pattern of the RX antenna [17]. For the proposed STAR antenna architecture, there are two mutual coupling paths between each RX port and the TX port. Due to the rotational symmetry of the whole antenna, here we just show the two coupling paths from RX port #1 to the TX port, as shown in Fig. 2(a). Path #1 is the direct coupling path between the TX monopole and the vertical capacitively coupled feedline of the RX antenna, and Path #2 is the coupling path via the top hat of the TX monopole and the horizontal meandered section of the RX antenna. The length difference between path #1 and path #2 is around half a wavelength at 2.45 GHz, resulting in destructive interference that reduces the mutual coupling between the TX port and each RX port. As a result, the transmission coefficient between the TX port and each RX port is well depressed, to be lower than -18.3 dB from 2.4 to 2.5 GHz as can be observed from Fig. 2(b). The low mutual coupling between the TX antenna and individual RX sections alleviates the requirements of the power handling of the quadrifilar IC.

C. Feeding Network for the RX Antenna

A quadrifilar IC (RFMW RQF2500Q06) is used to excite the four ports of the RX antenna. The quadrifilar IC is suitable for ISM band and can provide excitation signals with four different
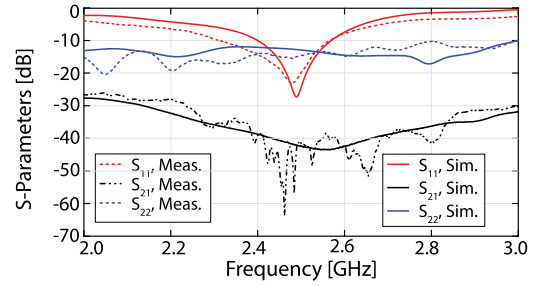

Fig. 3. Simulated and measured *S*-parameters of the proposed STAR antenna.

phase states of $0°$, $90°$, $180°$, and $270°$ at its four output ports. We soldered the quadrifilar IC on the feeding network [see Fig. 1(g)] and tested the phase and amplitude balance errors at the output ports of the feeding network. Measurement results show a maximum phase balance error of $7.1°$ and a maximum amplitude balance error of 0.9 dB over the frequency range of 2.4–2.6 GHz.

III. SIMULATION AND MEASUREMENT RESULTS

We conducted full-wave simulations of the STAR antenna using CST Microwave Studio to predict and optimize its performance. In the simulations, the TX antenna was excited with a waveguide port connected to the SMA connector at its input. The RX antenna was fed through four SMA connectors that are connected to a five-port data block representing the *S*-parameters of an ideal quadrifilar IC with perfect amplitude and phase balances. The simulated scattering parameters of the RX antenna were evaluated at the input port of this five-port data block. The dimensions of the TX and RX antennas were tuned to achieve good impedance matching, a high TX–RX isolation level, and omnidirectional radiation patterns with a vertical polarization. The finalized dimensions are given in Fig. 1. Subsequently, we fabricated the STAR antenna, as shown in Fig. 1(f). The RX antenna is connected to the feeding network by using four identical, 250 mm long coaxial cables. The input of the RX antenna is defined as the input port of the feeding network, as shown in Fig. 1(g). A vector network analyzer (Agilent N5225A) was used to measure the scattering parameters of the STAR antenna. All measured *S*-parameters were obtained inside a laboratory in a multipath environment.

Fig. 3 shows the simulated and measured scattering parameters of the TX and RX antennas of the fabricated prototype. The simulation results shown in Fig. 3 were obtained by combining the CST simulation results of the four-port RX antenna and the measured results of the feeding network to take into account the impact of the phase and amplitude imbalances of the fabricated feeding network on the predicted performance of the STAR antenna.[1] The measured impedance matching bandwidths (for $|S_{11}|$, $|S_{22}| \leq -10$ dB) of both TX and RX antennas show an overlapping region from 2.3 to 2.6 GHz, which is large enough to cover the 2.45 GHz ISM frequency band. The overlapped impedance-matching frequency range acquired from the measurements is slightly larger than the range of 2.4–2.6 GHz

---

[1]Note that the antenna was designed and optimized with an ideal feed network. The dimensions of the antenna were not changed to account for the nonideal response of the employed quadrifilar.
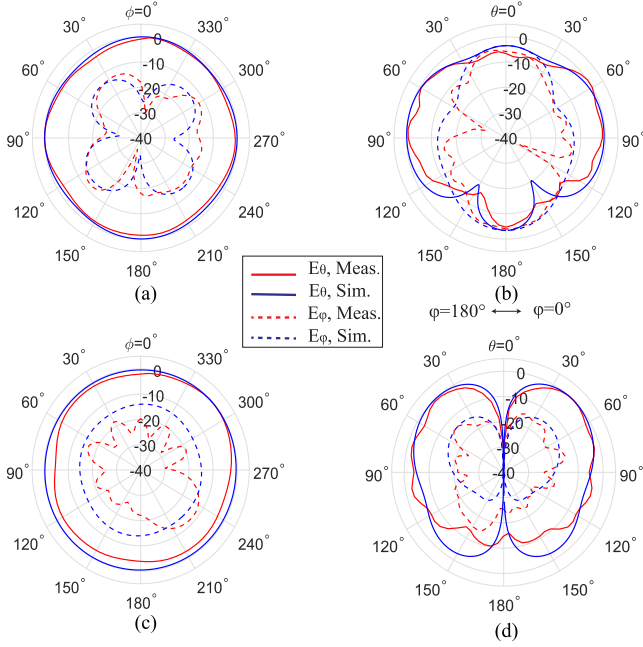
Fig. 4. Simulated and measured normalized 2-D radiation patterns of the STAR antenna at 2.45 GHz. (a) RX antenna along the azimuth plane (the xy plane). (b) RX antenna along the elevation plane (the xz plane). (c) TX antenna along the azimuth plane (the xy plane). (d) TX antenna along the elevation plane (the xz plane).

Fig. 5. Simulated and measured realized peak gains of the TX and RX antennas.

predicted in the simulations. The simulated isolation levels (as calculated from $|S_{21}|$ in Fig. 3) between the TX an RX antennas are more than 40 dB over the frequency range from 2.43 to 2.66 GHz with a peak value of 43 dB at 2.56 GHz, whereas the measured values are higher than 40 dB over almost the entire frequency range of 2.4–2.7 GHz with a peak value of 63 dB at 2.46 GHz. The small differences between the simulation and measurement results are mainly due to the fabrication and assembly tolerances of the antenna elements, imperfect amplitude and phase balances of the SMA connectors and four coaxial cables connecting the four RX ports and the outputs of the quadrifilar IC, and the impact of multipath propagation in the measurement environment. These discrepancies are expected to be further reduced if the STAR antenna is assembled in a higher precision, automated production process, and the ground plane and feeding network are integrated together in a multilayer printed circuit board.

The radiation patterns of the fabricated STAR antenna were measured using a multiprobe, spherical near-field measurement system over a frequency range of 2.0–3.0 GHz. When the RX antenna was measured, the input port of the TX antenna was terminated to 50 Ω, and vice versa. Due to rotational symmetry, the patterns of both the TX and RX antennas in the xz and yz planes are similar, and for brevity, the patterns in the yz plane are not reported. Fig. 4 shows the simulation and measurement results for the normalized gain patterns of the TX and RX antennas in both azimuth (xy plane) and elevation planes (xz plane) at 2.45 GHz. It can be seen in Fig. 4(a) that the RX antenna shows good omnidirectional radiation with vertical polarization in the azimuth plane. The gain variation is less than 1.5 dB over $0°-360°$ range of ϕ for the RX antenna at 2.45 GHz in the measurements. The RX antenna shows radiation toward the
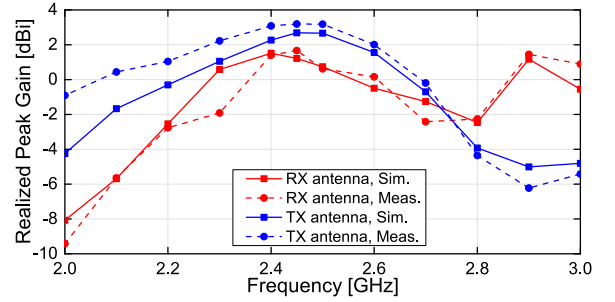
zenith direction, as shown in Fig. 4(b), which is mainly due to the limited size of the ground plane. A far-field null in the zenith direction could be achieved if an infinitely large ground plane is used. The simulated and measured radiation patterns of the TX antenna are shown in Fig. 4(c) and (d). The TX antenna shows a typical monopole-like radiation pattern with two axial nulls in the elevation plane and omnidirectional radiation patterns in the azimuth plane. The gain variation is smaller than 3.2 dB in the azimuth plane for the TX antenna at 2.45 GHz in the measurements. Overall, the simulation and measurement results agree reasonably well on the general shapes of the radiation patterns of both TX and RX antennas. The discrepancies in the normalized gain patterns between the simulated and measured results are mainly due to fabrication tolerances and measurement uncertainty. The simulated and measured realized peak gains of the TX and RX antennas are shown in Fig. 5. The reported gain values for both antennas include all of the losses in the feed network including the quadrifilar loss and the loss of coaxial cables used between the RX feed network and the input ports of the RX antenna. The simulation and measurement results show similar trends for the variation of the realized gain with respect to frequency for each antenna. Over the operating frequency range of 2.4–2.5 GHz, the measured realized peak gains of the TX and RX antennas range from 0.8–1.8 and 3.2–3.3 dBi, respectively.

IV. CONCLUSION

A vertically polarized STAR antenna with omnidirectional radiation in the azimuth plane was presented in this letter. The antenna system produces desirable radiation characteristics as well as a high TX–RX isolation level while being compact and low-profile. The RX antenna of this system is a capacitively fed cross loop, and the TX antenna is a top-hat-loaded monopole located at the center of the ground plane and aligned with the vertical symmetry axis of the RX antenna. The four ports of the RX antenna are fed with a quadrifilar IC to achieve a high TX–RX isolation level by utilizing the near-field cancellation technique. Meanwhile, we use the meandered horizontal strips of the cross loop of RX antenna to make the antenna compact and low-profile while producing a good vertical polarization. A prototype of the proposed antenna was fabricated and experimentally characterized. The prototype achieves an isolation level better than 38 dB between the TX and RX ports from 2.4 to 2.7 GHz, which covers the 2.45 GHz ISM band. Moreover, the antenna maintains consistent, monopole-like patterns for both TX and RX modes over the entire band of operation.

REFERENCES

[1] A. Sabharwal, P. Schniter, D. Guo, D. W. Bliss, S. Rangarajan, and R. Wichman, "In-band full-duplex wireless: Challenges and opportunities," *IEEE J. Sel. Areas Commun.*, vol. 32, no. 9, pp. 1637–1652, Sep. 2014.

[2] D. Bharadia and S. Katti, "Full duplex MIMO radios," in *Proc. USENIX NSDI*, Seattle, WA, USA, 2014, pp. 359–372.

[3] J. I. Choi, M. Jain, K. Srinivasan, P. Levis, and S. Katti, "Achieving single channel full duplex wireless communication," in *Proc. ACM MobiCom.*, Chicago, IL, USA, 2010, pp. 1–12.

[4] O. N. Alrabadi, A. D. Tatomirescu, M. B. Knudsen, P. Pelosi, and G. F. Pedersen, "Breaking the transmitter-receiver isolation barrier in mobile handsets with spatial duplexing," *IEEE Trans. Antennas Propag.*, vol. 61, no. 4, pp. 2241–2251, Apr. 2013.

[5] R. Lian, Z. Wang, Y. Yin, J. Wu, and X. Song, "Design of a low-profile dual-polarized stepped slot antenna array for base station," *IEEE Antennas Wireless Propag. Lett.*, vol. 15, pp. 362–365, 2016.

[6] H. Nawaz and I. Tekin, "Dual-polarized, differential fed microstrip patch antennas with very high interport isolation for full-duplex communication," *IEEE Trans. Antennas Propag.*, vol. 65, no. 12, pp. 7355–7360, Dec. 2017.

[7] E. Yetisir, C. C. Chen, and J. L. Volakis, "Wideband low profile multiport antenna with omnidirectional pattern and high isolation," *IEEE Trans. Antennas Propag.*, vol. 64, no. 9, pp. 3777–3786, Sep. 2016.

[8] Y. Li, Z. Zhang, W. Chen, Z. Feng, and M. F. Iskander, "A dual-polarization slot antenna using a compact CPW feeding structure," *IEEE Antennas Wireless Propag. Lett.*, vol. 9, pp. 191–194, 2010.

[9] A. T. Wegener and W. J. Chappell, "Simultaneous transmit and receive with a small planar array," in *IEEE/MTT-S Int. Microw. Symp. Dig.*, Montreal, QC, Canada, 2012, pp. 1–3.

[10] A. T. Wegener, "Broadband near-field filters for simultaneous transmit and receive in a small two-dimensional array," in *Proc. IEEE MTT-S Int. Microw. Symp.*, Tampa, FL, USA, 2014, pp. 1–3.

[11] D. Wu, S. W. Cheung, Q. L. Li, and T. I. Yuk, "Decoupling using diamond-shaped patterned ground resonator for small MIMO antennas," *Microw., Antennas Propag.*, vol. 11, no. 2, pp. 177–183, 2017.

[12] E. A. Etellisi, M. A. Elmansouri, and D. S. Filipovic, "Wideband monostatic simultaneous transmit and receive (STAR) antenna," *IEEE Trans. Antennas Propag.*, vol. 64, no. 1, pp. 6–15, Jan. 2016.

[13] E. A. Etellisi, M. A. Elmansouri, and D. S. Filipovic, "Wideband multimode monostatic spiral antenna STAR subsystem," *IEEE Trans. Antennas Propag.*, vol. 65, no. 4, pp. 1845–1854, Apr. 2017.

[14] M. A. Elmansouri, A. J. Kee, and D. S. Filipovic, "Wideband antenna array for simultaneous transmit and receive (STAR) applications," *IEEE Antennas Wireless Propag. Lett.*, vol. 16, pp. 1277–1280, 2017.

[15] K. E. Kolodziej, P. T. Hurst, A. J. Fenn, and L. I. Parad, "Ring array antenna with optimized beamformer for simultaneous transmit and receive," in *Proc. IEEE Antennas Propag. Soc. Int. Symp.*, Chicago, IL, USA, Jul. 2012, pp. 1–2.

[16] A. J. Fenn, P. T. Hurst, J. S. Herd, K. E. Kolodziej, L. I. Parad, and H. Steyskal, "Simultaneous transmit and receive antenna system," U.S. Patent 20130106667A1, May 2, 2013.

[17] R. Lian, T. Y. Shih, Y. Yin, and N. Behdad, "A high-isolation, ultra-wideband simultaneous transmit and receive antenna with monopole-like radiation characteristics," *IEEE Trans. Antennas Propag.*, vol. 66, no. 2, pp. 1002–1007, Feb. 2018.

[18] K. Kolodziej and B. Perry, "Vehicle-mounted STAR antenna isolation performance," in *Proc. IEEE Int. Symp. Antennas Propag.*, Vancouver, BC, Canada, 2015, pp. 1602–1603.